Single-crystal-to-single-crystal transformation in hydrogen-bond-induced high-spin pseudopolymorphs from protonated cation salts with a π-extended spin crossover Fe(III)…

Murata, Suguru
Takahashi, Kazuyuki
Sakurai, Takahiro
Ohta, Hitoshi

(Citation)
Polyhedron,136:170-175

(Issue Date)
2017-11-04

(Resource Type)
journal article

(Version)
Accepted Manuscript

(URL)
https://hdl.handle.net/20.500.14094/90005555

Single-crystal-to-single-crystal Transformation in Hydrogen-bond-induced High-spin Pseudopolymorphs from Protonated Cation Salts with a π-extended Spin Crossover Fe(III) Complex Anion

Suguru Murata [a], Kazuyuki Takahashi [a,*], Takahiro Sakurai [b], Hitoshi Ohta [c]

[a] *Department of Chemistry, Kobe University, 1-1 Rokkodai-cho, Nada-ku, Kobe, Hyogo 657-8501, Japan*

[b] *Research Facility Center for Science and Technology, Kobe University, 1-1 Rokkodai-cho, Nada-ku, Kobe, Hyogo 657-8501, Japan*

[c] *Molecular Photoscience Research Center, Kobe University, 1-1 Rokkodai-cho, Nada-ku, Kobe, Hyogo 657-8501, Japan*

Corresponding Author. Tel. & fax: +81-78-803-5691. E-mail address: ktaka@crystal.kobe-u.ac.jp (K. Takahashi).

Abstract

Novel pseudopolymorphic Hdabco compounds with an Fe(III) complex anion, (Hdabco)[Fe(aznp)$_2$]·CH_2Cl_2 **1** and (Hdabco)[Fe(aznp)$_2$]·0.5H_2O **2** [dabco = 1,4-diazabicyclo[2.2.2]octane, H_2aznp = (2'-hydroxyphenylazo)-2-hydroxynaphthalene], were prepared and characterized. The magnetic susceptibility for **1** and **2** revealed that both complexes were in a high-spin (HS) state in the whole temperature range and exhibited weak ferromagnetic interactions below 40 K. The crystal structural analyses suggested that strong N-H···O hydrogen bonding interactions between the Hdabco cation and [Fe(aznp)$_2$] anion may induce the distortion of a coordination structure resulting in the HS complexes, whereas π-stacking interactions between the π-ligands in the [Fe(aznp)$_2$] anion and additional C-H···N hydrogen bonding interactions between the Hdabco cation and [Fe(aznp)$_2$] anion constructed a intermolecular interaction framework structure with one-dimensional channels. The thermogravimetry analysis for compound **1** indicated the adsorption of a water molecule took place after the desorption of a dichloromethane molecule. This transformation of **1** into **2** proved to proceed in a single-crystal-to-single-crystal way by powder X-ray diffractions and single crystal X-ray structural analysis.

Keywords: Protonated cation; Anionic spin-crossover complex; Hydrogen bonding; π-stacking interaction; Single-crystal-to-single-crystal transformation

1. Introduction

Spin crossover (SCO) phenomenon between a high-spin (HS) and low-spin (LS) states has aroused a great interest in not only scientific fundamentals but also potential applications such as display, memory, and sensing devices [1-5]. Since an SCO conversion can be induced by temperature, pressure, light, and chemicals, the development of multifunctional SCO materials lead to the possibility to tune electronic functionalities of a molecular solid by external stimuli. So far a number of researches have been devoted to the introduction of a mononuclear SCO cation into various anionic conducting and magnetic molecular components such as TCNQ [6-9] and metal dithiolene complexes [10-16] [TCNQ = 7,7,8,8-tetracyano-quinodimetahane, dmit = 4,5-dithiolato-1,3-dithiole-2-thione]. However, to the best of our knowledge, the introduction of a mononuclear SCO anion into the hybrid SCO compound has never been known, because anionic mononuclear SCO complexes are very rare.

Recently we discovered a novel family of anionic mononuclear SCO Fe(III) complexes

from ONO tridentate azo-bisphenolate derivatives [17,18]. Along this line, we aimed to prepare a multifunctional hybrid compound by combining the π-extended SCO $Fe(aznp)_2$ anion with a functional cation [H_2aznp = (2'-hydroxyphenylazo)-2-hydroxynaphthalene]. Protonated dabco compounds were well known to afford several ferroelectric materials as well as a number of dielectric materials originated from a proton transfer or molecular motion [19-23] [dabco = 1,4-diazabicyclo[2.2.2]octane]. Thus, we focused on mono-protonated Hdabco cation as a cationic functional molecular component. We also investigated the possibility to determine the position of proton which reflects the difference in basicity between the dabco and [$Fe(aznp)_2$] anion molecules. We report herein the preparation, physical properties, and crystal structures of the pseudopolymorphic Hdabco compounds (Hdabco)[$Fe(aznp)_2$]·CH_2Cl_2 **1** and (Hdabco)[$Fe(aznp)_2$]·0.5H_2O **2** along with the desolvate compound (Hdabco)[$Fe(aznp)_2$]·xH_2O (x = 0−0.5) **1'** from **1** (Fig. 1). Although the [$Fe(aznp)_2$] anions in compounds **1** and **2** were in the HS state, we found a single-crystal-to-single-crystal transformation of **1** into **2** and, moreover, the desorption and adsorption of water molecules in the hydrate compound. All these physical properties of the present Hdabco compounds may originate from intermolecular hydrogen bonding interactions between the Hdabco cation and [$Fe(aznp)_2$] anion.

2. Materials and methods

All chemicals were purchased and used without further purification. H_2aznp was prepared according to the procedure of the literature [18]. (Hdabco)BF_4 was obtained by mixing an aqueous HBF_4 solution with an acetonitrile solution of dabco.

2-1. Synthesis of Hdabco compounds

To a red solution of H_2aznp (500 mg, 1.89 mmol) in 15 mL of methanol was added dropwise a methanol solution of sodium methoxide (4.16 mmol) at 60 ˚C. The solution turned to be dark violet. After stirring for 1.5 hours, to this solution was added a solution of $FeCl_3$ (156 mg, 0.96 mmol) in 9 mL of methanol and then stirred for 1 hour. To the solution was added corresponding (Hdabco)BF_4 (474 mg, 2.37 mmol) in 15 mL of methanol. After evaporating, the residue was washed by water and dried in vacuo. 598 mg of crude salt was obtained.

(Hdabco)[Fe(aznp)$_2$]·CH_2Cl_2 (**1**): Recrystallization of 606 mg of the crude salt from

dichloromethane-diethyl ether gave 274 mg of **1** as black platelets. Anal. Calcd. For $C_{39}H_{35}FeN_6O_4Cl_2$: C, 60.17; H, 4.53; N, 10.80%. Found: C, 60.34; H, 4.69; N, 10.69%.

(Hdabco)[Fe(aznp)$_2$]·xH_2O (**1'**): Heating the crystals of **1** to 200 °C and then cooling to room temperature gave **1'** as black platelets. Anal. Calcd. For $C_{38}H_{34}FeN_6O_{4.5}$ (x = 0.5): C, 64.96; H, 4.88; N, 11.96%. Found: C, 64.67; H, 4.86; N, 11.82%.

(Hdabco)[Fe(aznp)$_2$]·0.5H_2O (**2**): Recrystallization of 13.3 mg of the crude salt from acetonitrile-diethyl ether gave 5.6 mg of **2** as black platelets.

2-2. Physical measurements

The powder X-ray diffractions (PXRD) were performed using a RIGAKU SmartLab X-ray diffractometer with monochromated Cu-*K*α radiation. The TG-DTA was performed using a Rigaku TG8120 analyzer with a scan speed of 5 K mol^{-1}. Variable temperature direct current magnetic susceptibilities for aluminum-foil-wrapped polycrystalline samples (ca. 5-10 mg) sealed in a gelatin capsule were measured on a Quantum Design MPMS-XL magnetometer under a field of 0.5 T at a sweep speed of 2 K min^{-1} in the temperature range of 2−300 K. The sample

magnetization data were obtained by the subtraction of background magnetization data for the same gelatin capsule and aluminum foil from the measured data, and then the magnetic susceptibilities were corrected for diamagnetic contributions estimated by the magnetic susceptibility of each molecular component.

2-3. X-ray data collections and refinement

A crystal was mounted in a polyimide loop. All data were collected on a Bruker APEX II CCD area detector with monochromated Mo-*K*α radiation generated by a Bruker Turbo X-ray Source coupled with Helios multilayer optics. All data collections and calculations were performed using the APEX2 crystallographic software package (Bruker AXS). The data were collected to a maximum 2θ value of 55.0º. A total of 720 oscillation images were collected. The APEX II program was used to determine the unit cell parameters and for data collection. Data were integrated by using SAINT. Numerical absorption correction was applied by using SADABS. The structures at all temperatures were solved by direct methods and refined by full-matrix least-squares methods based on F^2 by using the SHELXTL program. All non-hydrogen atoms were refined anisotropically.

Hydrogen atoms were generated by calculation and refined using the riding model. Since the solvate CH_2Cl_2 molecule in the crystal of **1** was heavily disordered, the SQUEEZE method was applied to the refinement of the crystal structure.

3. Results and discussion

3.1. Synthesis of compounds **1** and **2**

The starting Hdabco salt was prepared by the metathesis reaction of the *in situ* generated $Na[Fe(aznp)_2]$ complex and $(Hdabco)BF_4$ in a methanol solution. Recrystallization from dichloromethane-diethyl ether gave a CH_2Cl_2-solvate complex **1**, while recrystallization from acetonitrile-diethyl ether afforded a hydrate complex **2**. Unfortunately, the preparation of **2** was not reproducible despite various attempts on crystallization conditions. On the other hand, a hydrate complex was unexpectedly obtained by heating the crystals of **1** to 200 °C and then cooling to room temperature, which is designated as desolvate complex **1'**. The compositions of both complexes **1** and **1'** were confirmed by thermogravimetry (TG) analysis, microanalysis, and single-crystal X-ray

structural analyses. The composition of **2** was also determined by single-crystal X-ray structural analysis.

3.2 Thermogravimetry-differential thermal analysis (TG-DTA)

To investigate thermal stability of the solvate compound **1**, TG-DTA was performed using a Rigaku TG8120 analyzer. The TG curves are shown in Fig. 2. On heating compound **1**, the weight loss started at around room temperature. The decrease in weight was very gradual and then the weight loss rate increased at 170 ˚C. Further heating resulted in a plateau of weight loss curve above 185 ˚C. The weight loss at 200 ˚C exactly corresponded to the weight ratio of one dichloromethane molecule (10.9%). After the above TG-DTA measurement we found the desolvate crystals **1'** retained their crystallinity at room temperature. Thus, TG-DTA for the sample **1'** was carried out again. Interestingly, the weight loss for **1'** was observed. The weight for **1'** decreased more rapidly and then was almost constant above 95 ˚C. The weight loss reached to 0.9% at 180 ˚C. The weight loss was consistent with the release of one half water molecule (1.28%) from compound **1'**. The water desorption and adsorption cycles were reproducible, while the absorption amount of water molecules was sensitive to humidity.

145

146 3.3 Powder X-ray Diffractions

147 To confirm the crystal structural changes upon heating the sample of **1**, the powder X-ray
148 diffractions (PXRD) were carried out using a RIGAKU SmartLab X-ray diffractometer. The PXRD
149 patterns for compounds **1** and **1'** along with the simulated patterns from the corresponding crystal
150 structural data for **1** and **2** described in the following section are shown in Fig. 3. The observed
151 diffraction patterns for the CH_2Cl_2-solvate compound **1** were the combination of the simulated
152 diffraction patterns for **1** and **2**, suggesting that desolvation took place during the measurement.
153 This observation is in good agreement with the decrease in weight of **1** even at room temperature.
154 On the other hand, the patterns for the desolvate sample of **1'** were completely different from those
155 for the parent CH_2Cl_2-solvate compound **1**, whereas those exactly corresponded to the simulated
156 patterns for the hydrate compound **2**. This means that a crystal-to-crystal structural transformation
157 of the CH_2Cl_2-solvate compound **1** into hydrate compound **2** through desolvate compound **1'**
158 occurred.

159

160 3.4. Crystal Structures for **1**, 1' and **2** ~~at 296 K~~

Single crystal X-ray structural analyses for **1**, **1'**, and **2** were performed using a Bruker AXS APEXII Ultra diffractometer. Fortunately, it was successful to determine the crystal structure of the desolvate compound **1'** despite a poor quality of crystal. Crystallographic data are listed in Table 2. All the crystal structures at 296 K were isostructural and belonged to monoclinic system with *C*2/*c*. The asymmetric units for all compounds contained one Hdabco cation and one [Fe(aznp)$_2$] anion from the following discussion about the structure of a dabco molecule (Fig. 4). In addition, one half water molecule was found for **1'** and **2**, whereas the CH_2Cl_2 molecule for **1** was heavily disordered and could not be assigned. Thus, the SQUEEZE treatment for the solvate CH_2Cl_2 molecule was applied for the refinement of crystal structure of **1**.

It is known that the C-N bond lengths are varied by protonation on the nitrogen atom in a dabco molecule. The C-N bond lengths for the present complexes along with the proton-ordered Hdabco [24] and H_2dabco [25] compounds are shown in Table 3. The average C-N bond lengths including the N5 atom in the vicinity of the coordination core of the [Fe(aznp)$_2$] anion were 0.03 Å longer than those including the N6 atom on the other side in all the Hdabco salts. This clearly indicates that mono-protonation occurred only on the N5 atom in the vicinity of the coordination

177 core. Moreover, the intermolecular distance between N5 and O1 atoms in the [Fe(aznp)$_2$] anion was
178 2.680(5) Å, indicative of strong hydrogen bonding interactions between them. In addition, weak
179 hydrogen bonding interactions of 3.05(3) and 3.048(8) Å between the hydrate water molecule and
180 non-protonated nitrogen atom in the Hdabco molecule were found for desolvate compound **1'** and
181 hydrate compound **2**, respectively.

182 The π-ligand aznp molecule was coordinated to a central Fe atom as a tridentate chelate
183 ligand and thus two coordinated ligand molecules were arranged in an almost perpendicular manner
184 (Figure 4). There was no orientational disorder of the aznp ligand unlike the mother anionic SCO
185 Fe(III) complexes [17]. The bond lengths of the aznp ligand were unchanged from those of the
186 previous [Fe(aznp)$_2$] complexes [18], suggesting that the charge transfer from the aznp ligand to
187 Fe(III) ion did not occur. The selected coordination bond lengths and distortion parameters are
188 given in Table 3. As compared with the coordination bond lengths of HS (TMA)[Fe(aznp)$_2$] [18],
189 the Fe-O1 and Fe-O2 bond lengths in the Hdabco salts were about 0.05 Å longer and 0.02 Å shorter,
190 respectively, whereas the Fe-O3, Fe-O4, and Fe-N bond lengths were similar. These variations
191 would arise from the strong hydrogen bonding between O1 and N5 atoms. Note that the distortion
192 parameters in the present Hdabco compounds were extremely larger than those in the HS

193 [Fe(aznp)$_2$] complexes reported previously [18]. Thus, the distortion of a coordination structure
194 would originate from this strong N-H···O hydrogen bonding between the aznp ligand and Hdabco
195 cation. All these coordination structural features indicated that all present Hdabco compounds were
196 in the HS state, which were consistent with the following magnetic susceptibility data.

197 The molecular arrangements of the [Fe(aznp)$_2$] anion in **2** are shown in Fig. 5a. The
198 naphthalene ring in an Fe(aznp)$_2$ anion overlapped those in the neighboring anions in two kinds of
199 overlapping modes (Fig. 5b). One molecular overlapping mode (*p*) was parallel to each other and
200 the π-plane distance was 3.46 Å for **1**. The other one (*q*) was not parallel and the short C···C
201 contact was 3.66 Å for **1**. These two kinds of π-stacking interactions between the naphthalene rings
202 formed a π-stacking tetramer in an Np···*q*···Np···*p*···Np···*q*···Np manner (Np represents
203 naphthalene ring). The opposite π-ligand to the π-stacking ligand in the central π-stacking dimer
204 (Np···*p*···Np) was involved in the end of the neighboring π-stacking tetramer, thus each tetramer
205 was arranged in an almost perpendicular manner and formed the two-dimensional π-stacking
206 sheet-like structure parallel to the *bc* plane. On the other hand, the corresponding short π-contact
207 distances of *p* and *q* for **2** were 3.73 and 3.55 Å, respectively. This suggests that the crystal
208 structural transformation might reduce π-stacking interactions between the [Fe(aznp)$_2$] anions.

The two-dimensional π-stacking sheet-like structures in **2** were bridged by the H-N^+-C-H···O hydrogen bonding interactions [26] with a C33···O3 distance of 3.116(6) Å, resulting in the formation of a one-dimensional (1D) channel along the *b* axis (Fig. 5c). The water molecules were bound in the one-dimensional channel by weak hydrogen bonding interactions between the oxygen atom of a solvate water molecule and non-protonated nitrogen atom of an Hdabco molecule. The similar 1D channel structure was found in **1**, where the disordered CH_2Cl_2 molecule should exist. The calculated sizes per the asymmetric unit of the void exclusive of the solvent molecule for **1**, **1'**,and **2** were 146, 48.3, and 41.6 $Å^3$, respectively. Thus, the CH_2Cl_2 molecules could be released without collapsing the crystallinity of **1** (Fig.5d), whereas the desolvated crystals **1'** can absorb only a water molecule in the channel. The C33···O3 distance for **1** was slightly shortened to be 3.077(6) Å. Since the hydrate water molecule in **1'** can be easily desorbed from the channel, the retainment of the 1D channel structure after desolvation could be attributed to the C-H···O hydrogen bonding between the two-dimensional π-stacking networks.

3.5. Magnetic susceptibility for **1** and **2**

The temperature dependence of magnetic susceptibilities for **1** and **2** is shown in Fig. 6. The $\chi_M T$ values for **1** and **2** at 300 K were 4.42 and 4.44 cm^3 K mol^{-1}, respectively. Thus, the central Fe(III) ion for both compounds were in the HS state. On lowering the temperature, the $\chi_M T$ values were almost constant and then slight increase in $\chi_M T$ was observed below 40 K, indicative of the existence of a ferromagnetic interaction. Fitting of the $\chi_M T$ vs. T products by the Curie-Weiss law in the temperature range of 15-50 K gave C = 4.32 cm^3 K mol^{-1} with θ = 0.18 K for **1** and C = 4.36 cm^3 K mol^{-1} with θ = 0.44 K for **2**. Although one of the previous [Fe(aznp)$_2$] compounds showed a SCO conversion [18], the present compounds did not show an SCO phenomenon. The structural comparison of the previous and present [Fe(aznp)$_2$] compounds described in the crystal structures section along with no notable structural change in **1'** at 90 K indicates that the remarkable distortion of a coordination structure gives rise to the HS state, which comes mainly from the strong N-H···O hydrogen bonding interactions between the Hdabco cation and [Fe(aznp)$_2$] anion. Concerning the weak ferromagnetic interactions, since similar weak magnetic interactions through π-staking interactions were reported in the related Fe(III) complex exhibiting the antiferromagnetic transition at very low temperature [28], we assumed the possibility of an exchange coupling path through π-stacking interactions of the central π-dimer (Fig. 5b, overlap *p*) according to the McConnell-I

mechanism [27]., because the antiferromagnetic transition through π-staking interactions at very low temperature in the related Fe(III) complex [27].

4. Conclusion

We have prepared novel pseudopolymorphic Hdabco compounds **1** and **2** with the SCO $[Fe(aznp)_2]$ anion. The magnetic susceptibility and crystal structural analysis revealed that **1** and **2** were in the HS state due to the distortion of a coordination structure by the strong N-H···O hydrogen bonding interaction between the proton on the dabco molecule and the oxygen atom of the anzp ligand. The structural comparison between the CH_2Cl_2-solvate and hydrate compounds indicated the H-N^+-C-H···O hydrogen bonding between the two-dimensional π-stacking interaction networks may play a key role in the construction of the one-dimensional channel structure, resulting in the occurrence of the single-crystal-to-single-crystal (SCSC) structural transformation and the ability of desorption and adsorption of water molecules in the present molecular system. Since several SCO compounds showing the solvent-induced SCSC transformation were recently reported [29-33], the present founding give an insight into the design of new solvent-induced SCSC SCO

compounds.

Supplementary data

CCDC 1527225-1527227 and 1539769 contain the supplementary crystallographic data for this paper. These data can be obtained free of charge via http://www.ccdc.cam.ac.uk/conts/retrieving.html, or from the Cambridge Crystallographic Data Centre, 12 Union Road, Cambridge CB2 1EZ, UK; fax: (+44) 1223-336-033; or e-mail: deposit@ccdc.cam.ac.uk.

Acknowledgements

This work was partially supported by JSPS KAKENHI Grant Number 25410068.

References

[1] P. Gütlich, H.A. Goodwin (Eds.), Spin Crossover in Transition Metal Compounds I-III, Topics in Current Chemistry 233-235, Springer, Berlin, 2004.

[2] M.A. Halcrow (Ed.), Spin-Crossover Materials, John Wiley & Sons, Ltd.: Oxford, United Kingdom, 2013.

[3] A. Bousseksou, G. Molnár, L. Salmon, W. Nicolazzi, Chem. Soc. Rev. 40 (2011) 3313-3335.

[4] P. G. Lacroix, I. Malfant, J.-A. Real, V. Rodriguez, Eur. J. Inorg. Chem. (2013) 615-627.

[5] P. Gütlich, A. B. Gaspar, Y. Garcia, Beilstein J. Org. Chem. 9 (2013) 342-391.

[6] M. Nakano, N. Fujita, G. Matsubayashi, W. Mori, Mol. Cryst. Liq. Cryst. 379 (2002) 365-370.

[7] H. Phan, S. M. Benjamin, E. Steven, J. S. Brooks, M. Shatruk, Angew. Chem. Int. Ed. 54 (2015) 823-827.

[8] X. Zhang, Z.-X. Wang, H. Xie, M.-X. Li, T.J. Woods, K.R. Dunbar, Chem. Sci. 7 (2016) 1569-1574.

[9] K. Takahashi, H.-B. Cui, H. Kobayashi, Y. Einaga, O. Sato, Chem. Lett. 34 (2005) 1240-1241.

[10] K. Takahashi, H.-B. Cui, Y. Okano, H. Kobayashi, Y. Einaga, O. Sato, Inorg. Chem. 45 (2006) 5739-5741.

[11] K. Takahashi, H.-B. Cui, Y. Okano, H. Kobayashi, H. Mori, H. Tajima, Y. Einaga, O. Sato, J. Am. Chem. Soc. 130 (2008) 6688-6689.

[12] A.I.S. Neves, J.C. Dias, B.J.C. Vieira, I.C. Santos, M.B. Castelo Branco, L.C.J. Pereira, J.C.

289 Waerenborgh, M. Almeida, D. Belo, V. da Gama, CrystEngComm 11 (2009) 2160-2168.

290 [13] K. Takahashi, H. Mori, H. Kobayashi, O. Sato, Polyhedron 28 (2009) 1776-1781.

291 [14] M. Nihei, H. Tahira, N. Takahashi, Y. Otake, Y. Yamamura, K. Saito, H Oshio, J. Am. Chem.

292 Soc. 132 (2010) 3553-3560.

293 [15] K. Fukuroi, K. Takahashi, T. Mochida, T. Sakurai, H. Ohta, T. Yamamoto, Y. Einaga, H. Mori,

294 Angew. Chem. Int. Ed. 53 (2014) 1983-1986.

295 [16] M. Okai, K. Takahashi, T. Sakurai, H. Ohta, T. Yamamoto, Y. Einaga, J. Mater. Chem. C 3

296 (2015) 7858-7864.

297 [17] K. Takahashi, K. Kawamukai, M. Okai, T. Mochida, T. Sakurai, H. Ohta, T. Yamamoto, Y.

298 Einaga, Y. Shiota, K. Yoshizawa, Chem. Eur. J. 22 (2016) 1253-1257.

299 [18] S. Murata, K. Takahashi, T. Sakurai, H. Ohta, T. Yamamoto, Y. Einaga, Y. Shiota, K.

300 Yoshizawa, Crystals 6 (2016) 49 (16 pages).

301 [19] A. Katrusiak, M. Szafrański, Phys. Rev. Lett. 88 (1999) 576-579.

302 [20] T. Akutagawa, S. Takeda, T. Hasegawa, T. Nakamura, J. Am. Chem. Soc. 126 (2004) 291-294.

303 [21] Y. Zhang, W. Zhang, S.-H. Li, Q. Ye, H.-L.Cai, F. Deng, R.-G. Xiong, S. D. Huang, J. Am.

304 Chem. Soc. 134 (2012) 11044-11049.

[22] W. Zhang, L.-Z. Chen, R.-G. Xiong, T. Nakamura, S. D. Huang, J. Am. Chem. Soc. 131 (2009) 12544-12545.

[23] Z.-S. Yao, K. Yamamoto, H.-L. Cai, K. Takahashi, and O. Sato, J. Am. Chem. Soc. 138 (2016) 12005-12008.

[24] M. Szafrański, Chem. Phys. Lett. 457 (2008) 110-114.

[25] L. Brammer, J. K. Swearingen, E. A. Bruton, P. Sherwood, Proc. Natl. Acad. Sci. USA, 99 (2002) 4956-4961.

[26] R. Taylor, O. Kennard, J. Am. Chem. Soc. 104 (1982) 5063-5070.

[27] K. Takahashi, K. Kawamukai, T. Mochida, T. Sakurai, H. Ohta, T. Yamamoto, Y. Einaga, H. Mori, Y. Shimura, T. Sakakibara, T. Fujisawa, A. Yamaguchi, A. Sumiyama, Chem. Lett. 44 (2015) 840-842.

[28] H. M. McConnell, J. Chem. Phys. 39 (1963) 1910.

[29] J. J. M. Amoore, C. J. Kepert, J. D. Cashion, B. Moubaraki, S. M. Neville, K. S. Murray, Chem. Eur. J. 12 (2006) 8220-8227.

[30] R.-J. Wei, J. Tao, R.-B. Huang, L.-S. Zheng, Inorg. Chem. 50 (2011) 8553-8564.

[31] J. S. Costa, S. Rodríguz-Jiménez, G. A. Craig, B. Barth, C. M. Beavers, S. J. Teat, G. Aromí, J.

Am. Chem. Soc. 136 (2014) 3869-3874.

[32] L. K. Cook, R. Kulmaczewski, O. Cespedes, M. A. Halcrow, Chem. Eur. J. 22 (2016) 1789-1799.

[33] R. G. Miller, S. Brooker, Chem. Sci. 7 (2016) 2501-2505.

Table 1. Summary of crystallographic data and refinement details for **1**, **1'**, and **2**.

Compound	**1**	**1'**		**2**
Temperature / K	296	296	90	296
Empirical formula	$C_{39}H_{35}FeN_6O_4Cl_2$	$C_{38}H_{34}FeN_6O_{4.5}$	$C_{38}H_{34}FeN_6O_{4.5}$	$C_{38}H_{34}FeN_6O_{4.5}$
Formula weight	778.48	702.56	702.56	702.56
Color	black	black	black	black
Dimension	0.27×0.14×0.02	0.25 × 0.11 × 0.03	0.40 × 0.28 × 0.05	0.35 × 0.27 × 0.03
Crystal system	Monoclinic	Monoclinic	Monoclinic	Monoclinic
Space group	*C*2/c	*C*2/c	*C*2/c	*C*2/c
a / Å	30.654(14)	27.582(10)	27.168(8)	27.619(6)
b / Å	12.309(5)	12.744(5)	12.686(4)	12.677(3)
c / Å	24.178(11)	22.741(13)	22.291(7)	22.655(5)
α / °	90	90	90	90
β / °	127.966(5)	122.083(3)	121.628(3)	122.082(2)
γ / °	90	90	90	90
V / Å^3	7192(5)	6773(5)	6542(3)	6721(3)
Z	8	8	8	8
ρ_{calcd} / g cm^{-3}	1.438	1.378	1.427	1.389
$2\rho_{max}$ / °	50.06	50.06	54.20	50.04
No. Reflections	16693	14214	16952	14930
(R_{int})	(0.0736)	(0.0856)	(0.0704)	(0.0599)
No. Observations	6363	5959	7154	5920
(I>2.00σ(I))	(3274)	(2700)	(4893)	(3245)
No.Variables	442	447	447	447
R_1 (I>2.00σ(I))	0.0630	0.1061	0.0807	0.0637
R_1 (all data)	0.1295	0.2059	0.1196	0.1325
wR_2 (I>2.00σ(I))	0.1532	0.1797	0.2017	0.1467
wR_2 (all data)	0.1854	0.2177	0.2226	0.1792
Goodness of fit	0.940	1.062	1.116	1.033

Table 2. C-N bond lengths of a dabco molecule for **1**, **1'**, **2**, and related dabco compounds.

	1	**1'**		**2**		(Hdabco) (HF_2)	(H_2dabco) ($CuCl_4$)	
T / K	296	296	90	296		300	296	
N5-C33 / Å	1.486(5)	1.488(9)	1.498(6)	1.482(6)	H^+N-C	1.484	1.493(4)	1.505(4)
N5-C35 / Å	1.474(6)	1.479(9)	1.497(6)	1.476(6)		1.484	1.486(4)	1.497(4)
N5-C37 / Å	1.478(6)	1.474(9)	1.505(6)	1.488(6)		1.486	1.487(4)	1.493(4)
Average Length / Å	1.479(6)	1.480(9)	1.500(6)	1.482(6)		1.485	1.489(4)	1.498(4)
N6-C34 / Å	1.455(6)	1.463(10)	1.467(7)	1.455(7)	N-C	1.457		
N6-C36 / Å	1.431(7)	1.444(11)	1.458(7)	1.437(7)		1.447		
N6-C38 / Å	1.452(7)	1.460(10)	1.484(7)	1.439(7)		1.447		
Average Length / Å	1.446(7)	1.456(10)	1.470(7)	1.444(7)		1.450		
	This work	This work	This work	This work		Ref. 23	Ref. 24	

Table 3. Selected bond lengths, angles, and the distortion parameters of **1**, **1'**, **2**, and related complex.

	1	**1'**		**2**	(TMA)[Fe(aznp)$_2$]·CH$_3$CN		(TMA)[Fe(aznp)$_2$]·(CH$_3$)$_2$C=O
T / K	296	296	90	296	90	273	90
Fe1-O1 / Å	2.014(3)	2.029(5)	2.027(3)	2.023(3)	1.913(3)	1.960(2)	1.999(3)
Fe1-O2 / Å	1.936(3)	1.951(5)	1.959(3)	1.952(3)	1.878(3)	1.965(3)	1.979(3)
Fe1-N1 / Å	2.111(4)	2.127(6)	2.128(4)	2.119(4)	1.952(3)	2.110(2)	2.161(3)
Fe1-O3 / Å	1.954(3)	1.982(5)	1.985(3)	1.980(3)	1.936(3)	1.975(3)	1.994(2)
Fe1-O4 / Å	1.965(3)	1.976(5)	1.979(3)	1.969(3)	1.884(4)	1.969(3)	1.983(2)
Fe1-N3 / Å	2.160(4)	2.171(6)	2.162(4)	2.161(4)	1.967(4)	2.136(3)	2.156(3)
Σ^1 / °	117.18(13)	127.5(2)	131.85(14)	129.28(13)	27.63(15)	80.24(11)	99.67(10)
Θ^2 / °	209.46(11)	230.40(18)	237.50(12)	233.85(12)	46.72(13)	151.24(9)	185.12(9)
	This work	This work	This work	This work	Ref. 18	Ref. 18	Ref. 18

[1] The sum of the absolute differences of bite angles from 90°. [2] The sum of the absolute differences of all the angles of triangle surfaces of a coordination octahedron from 60°.

Table 4. Selected intermolecular distances involving hydrogen bonding and π-stacking interactions for **1**, **1'**, and **2** at 296 K

	1	**1'**		**2**
T / K	296	296	90	296
Hydrogen Bonding				
O1···H–N5 / Å (ligand···cation)	2.680(5)	2.663(7)	2.652(5)	2.656(5)
N6···H–O5 / Å (cation···H_2O)	–	3.05(3)	2.972(6)	3.048(8)
C33–H···O3 (cation···ligand)	3.077(6)	3.131(9)	3.028(6)	3.116(6)
π-stacking				
π-distance (*p*) / Å	3.459	3.738	3.691	3.730
short C···C (*q*) / Å	3.655	3.537	3.518	3.545

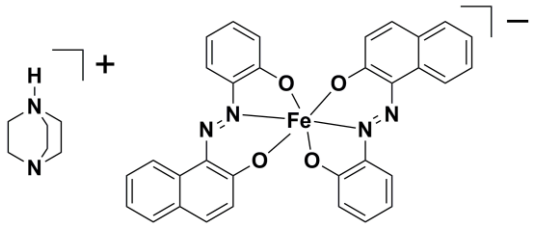

Fig. 1. Molecular structure of (Hdabco)[Fe(aznp)$_2$].

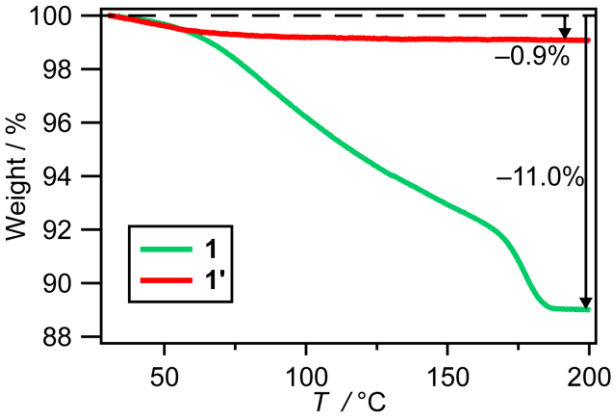

Fig. 2. TG curves for **1** and **1'**.

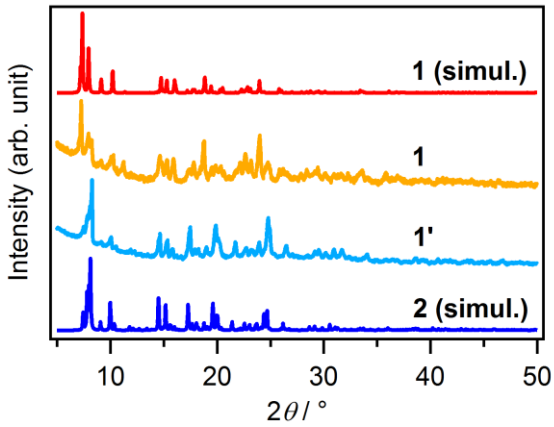

Fig. 3. Measured and simulated powder X-ray diffraction patterns for **1**, **1'**, and **2**.

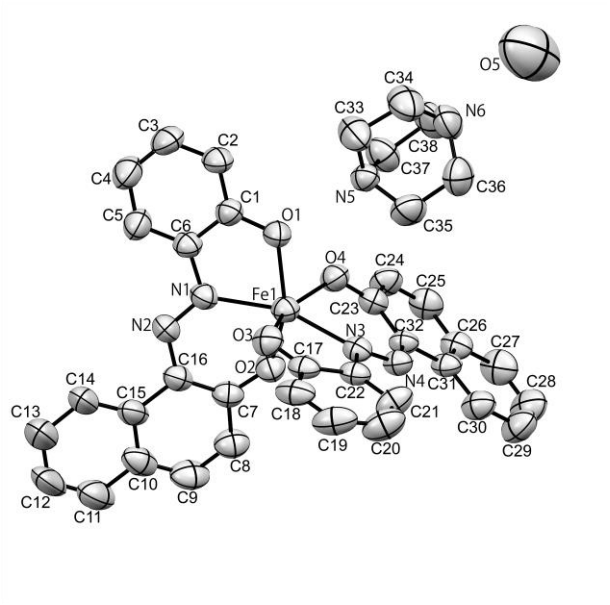

Fig. 4. ORTEP drawings (50% probability) of the molecular structures and numbering schemes for **2**.

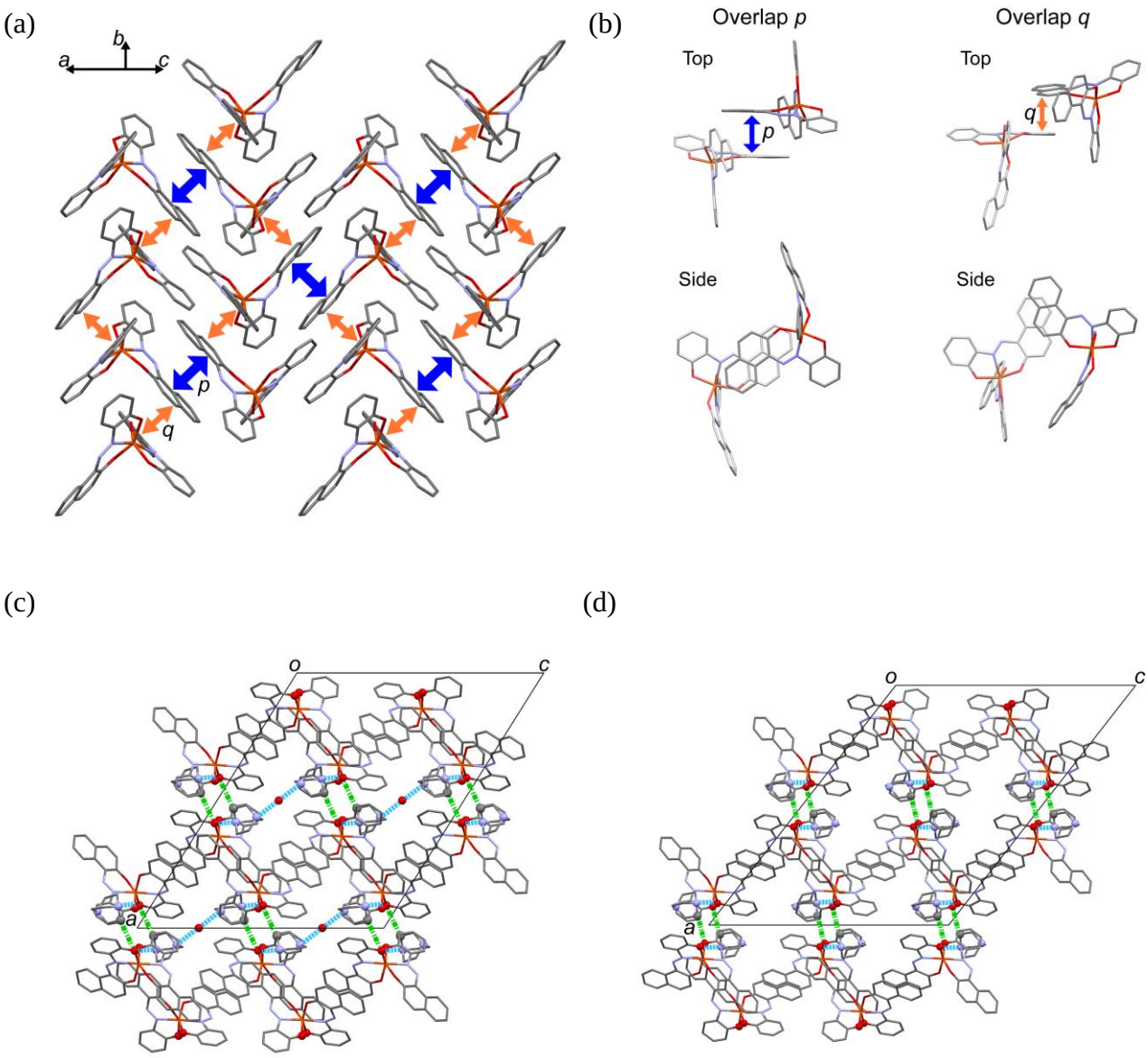

Fig. 5. (a) π-stacking structure for **2**. Double-headed arrows *p* and *q* indicate the same overlapping modes. (b) Top and side views for each π-overlapping mode for **2**. (c) Crystal structure of **2** viewed along the *b* axis. (d) Crystal structure of **1** viewed along the *b* axis. Blue and green dot lines indicate the O-H···N and C-H···O hydrogen bonding interactions, respectively.

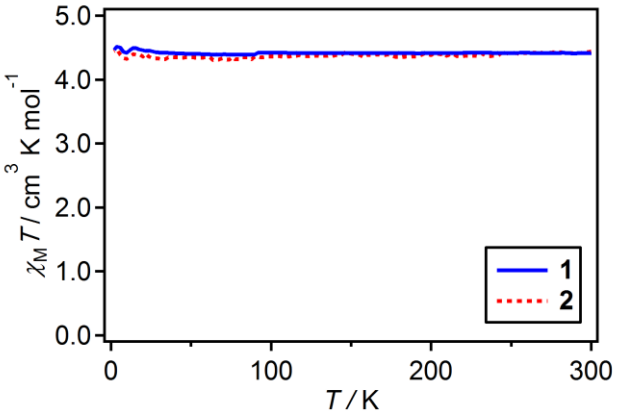

Fig. 6. The χ_M vs. T products for **1** and **2**.